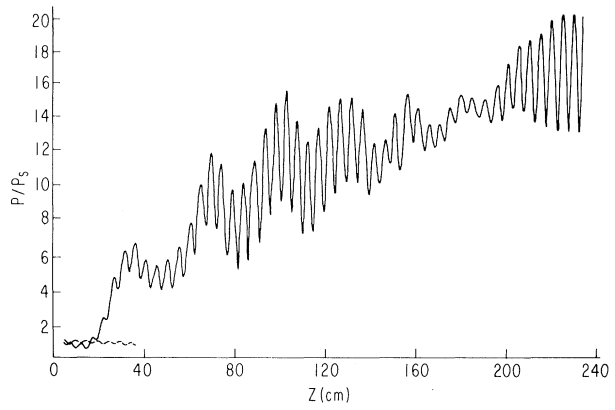

FIG. 5. Wave power (linear scale) vs axial distance. The launched wave amplitude is near the saturation level which is marked by the dashed line. $V_0 = 55.7$ V, $I_0 = 0.50$ mA, $f = 45.0$ MHz, $E_{dc} = 1.88$ V/cm, and $P_s = 5.36$ mW. The applied static voltage $V_H = 506$ V.

static electric field on beam trapping in a TWT. For weak fields the wave power can be enhanced while for stronger fields beam detrapping occurs and the enhancement diminishes. Space charge can play an important role in causing the beam to be detrapped. The wave enhancement has been found to be strongly dependent on the rf input drive level. In particular, appreciable wave enhancement of launched large-amplitude waves has been observed.

We wish to thank Professor N. M. Kroll for useful discussions. This work was supported by the National Science Foundation under Grant No. PHY80-09326.

[1]G. J. Morales, Phys. Rev. Lett. 41, 646 (1978).
[2]J. R. Pierce, *Traveling Wave Tubes* (Van Nostrand, New York, 1950).
[3]P. K. Tien, Bell Sys. Tech. J. 35, 349 (1956).
[4]T. M. O'Neil, J. H. Winfrey, and J. H. Malmberg, Phys. Fluids 14, 1204 (1971); T. M. O'Neil and J. H. Winfrey, Phys. Fluids 15, 1514 (1972).
[5]I. N. Onischenko, A. R. Linetskii, N. G. Matsiborko, V. D. Shapiro, and V. I. Shevchenko, Pis'ma Zh. Eksp. Teor. Fiz. 12, 407 (1970) [JETP Lett. 12, 281 (1970)].
[6]R. L. Hess, Ph.D. thesis, University of California, 1960 (unpublished).
[7]J. E. Rowe, *Nonlinear Electron-Wave Interaction Phenomena* (Academic, New York, 1965).
[8]N. M. Kroll, P. Morton, and M. N. Rosenbluth, *Free Electron Generators of Coherent Radiation* (Addison-Wesley, Reading, Mass., 1980), Chaps. 4, 5, and 6.
[9]G. Dimonte and J. H. Malmberg, Phys. Fluids 21, 1188 (1978).

Measurements of Enhanced Stopping of 1-MeV Deuterons in Target-Ablation Plasmas

F. C. Young, D. Mosher, S. J. Stephanakis, and Shyke A. Goldstein[a]
Naval Research Laboratory, Washington, D. C. 20375

and

T. A. Mehlhorn
Sandia National Laboratory, Albuquerque, New Mexico 87115
(Received 28 April 1982)

Enhancement of the energy loss of 1-MeV deuterons in target-ablation plasmas over that in cold targets has been observed when signficant ionization is present in the plasma. Scaling of enhanced stopping with target ionization is consistent with stopping by free electrons and the remaining bound electrons. Measured energy losses for Mylar and aluminum targets are also in agreement with hydrocode calculations.

PACS numbers: 52.40.Mj, 29.70.Gn, 52.50.Gj, 52.70.Nc

Inertial confinement fusion (ICF) with ion-beam drivers requires high-power-density deposition of ion energy in fusion targets. The beam power density is proportional to the current density focused onto the pellet target and to the stopping power of the beam-heated target material. Calculations[1-3] indicate that at the ionization levels of ICF pellet plasmas, the ion stopping power is enhanced such that the ion range is about half of that in a cold target. In this paper, measurements of the energy loss of megaelectronvolt deuterons in plasmas formed by focusing the beam

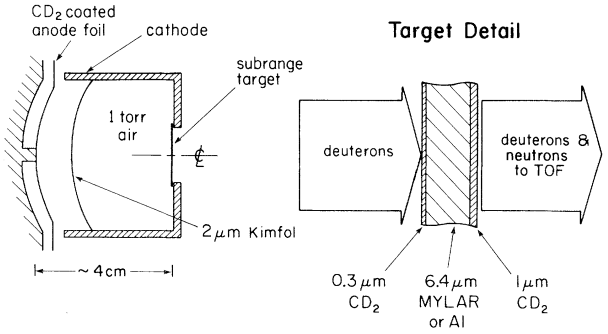

FIG. 1. Conceptual experimental schematic.

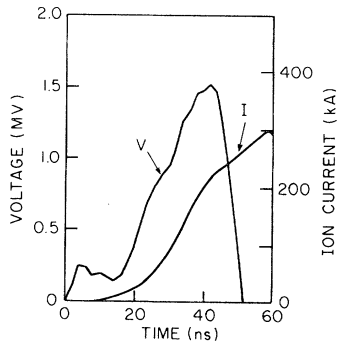

FIG. 2. Diode-voltage and ion-current traces.

(1 MeV, 0.2 MA, 20 ns) onto subrange-thick targets are presented. The results demonstrate that the stopping power is enhanced and confirm theoretical scaling of the stopping power with target ionization.

Recent pulsed-power and diode-physics advances have resulted in the focusing of proton and deuteron beams to several hundred kiloamperes per square centimeter, sufficient for experiments on ion stopping in plasmas.[4] For the present energy-loss experiments, a pinch-reflex diode,[4,5] operating at a peak voltage of about 1.5 MV, is used to produce an intense deuteron beam. A 6-cm-diam annular cathode is employed, and a 100-μm-thick plastic anode, coated with deuterated polyethylene (CD_2), provides the deuteron beam. The ion beam is charge and current neutralized by a 1.8-μm-thick polycarbonate foil at the cathode and 1 Torr air in the focusing-drift region (Fig. 1). The ion current passing through this foil is measured by a Rogowski coil. Typical corrected-voltage and ion-current traces are shown in Fig. 2. After about 40 ns into the pulse, the voltage decreases abruptly due to insulator flashover. Both planar and spherically contoured anodes[4] are used to produce different beam-current densities on target in order to vary target heating. With planar anodes, the beam focus in 10–15 cm from the anode. With spherical anodes, higher current density is achieved about 4 cm from the anode apex.

The experimental technique for determining the deuteron energy loss uses neutron time-of-flight (TOF) with multilayered targets.[6] The beam is focused onto a target consisting of a 6.4-μm-thick subrange stopping foil of Mylar or aluminum sandwiched between 0.3- and 1.0-μm-thick layers of CD_2 (Fig. 1). The TOF of d-d neutrons from the two CD_2 targets determines both the incident deuteron energy and the energy loss in the stopping foil. Neutrons are detected in the forward beam direction, and reaction kinematics[7] are used to extract deuteron energies. Neutrons from the two CD_2 targets are time resolved for a 7.6-m neutron flight path. For planar diodes, the time separation of neutrons from the two targets is increased by locating the rear CD_2 target 21 cm behind the front CD_2 target and stopping foil.

A typical trace from the TOF detector is shown in Fig. 3. The response time (full width at half maximum) of this detector is 4 ns, and its output is linear to 15 V. Bremsstrahlung from the diode saturates the detector, but the neutron pulses are TOF delayed and resolved about 260 ns after the bremsstrahlung pulse. Measurements with just a front or a rear CD_2 target confirm that this neutron response is the superposition of neutrons

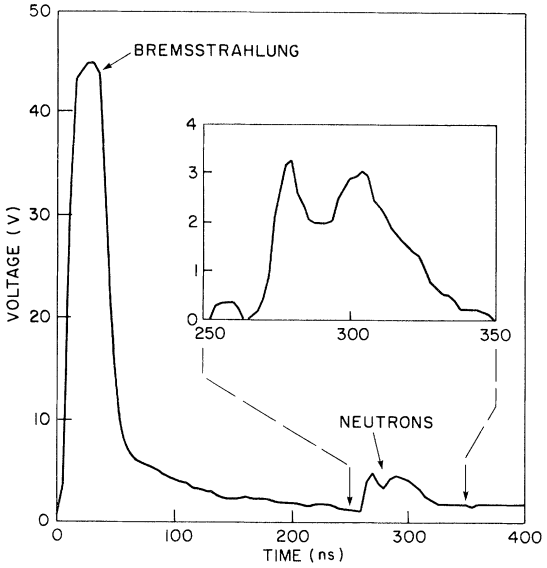

FIG. 3. Neutron TOF trace measured with a Mylar stopping foil and spherical diode.

from the front target (first neutron pulse) and the back target (second neutron pulse), respectively. The bremsstrahlung tail has been subtracted from the neutron signal shown in the inset. Since the neutron output is maximum at peak ion power, the time interval between peak ion power and the peak of the first neutron pulse determines the neutron energy from the front CD_2 target and, by kinematics, the incident deuteron energy. The deuteron energy is determined from the neutron energy and neutron emission angle relative to the deuteron direction. For planar (spherical) diodes, this angle ranges from 0° to about 10° (40°) from the target normal so that an average angle of 5° (20°) is used. A small correction ($\leq 5\%$) is made to the neutron TOF for the TOF of deuterons from the anode to the target. The time separation of the two neutron peaks provides a direct measure of the deuteron energy loss in the stopping foil. This time interval is corrected for the TOF of deuterons from the front to the rear CD_2 target in planar-diode measurements.

Results of energy-loss measurements are presented in Fig. 4. For planar diodes, horizontal errors of ± 0.11 MeV arise from an uncertainty of ± 4 ns in timing neutron signals relative to the peak ion power. Vertical errors of ± 50 keV result from an uncertainty of ± 3 ns in the separation of the two neutron peaks. For spherical diodes, the horizontal and vertical errors include uncertainties due to the large range of deuteron angles on target. Cold-target energy losses, deduced from stopping cross sections[8] using the average angles, are compared with the measurements in Fig. 4. Measured energy losses are significantly larger than cold-target values except for the planar diode with a Mylar target. In that case, measurements are consistent with cold-target values.

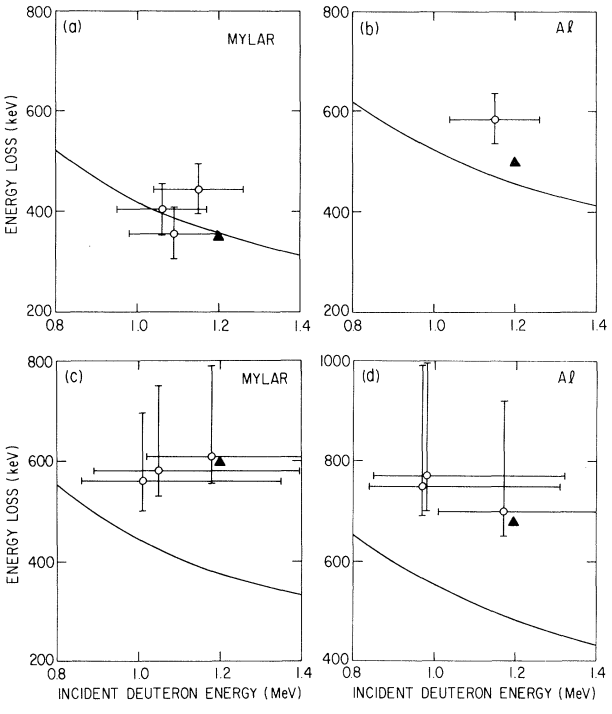

FIG. 4. Comparison of energy-loss measurements for (a) and (b) planar and (c) and (d) spherical diodes with energy-loss curves calculated for solid targets. The triangles are hydrocode results.

The ion-current density on target is required to evaluate target heating. Proton beam-current densities were determined by measuring K-line radiation from aluminum targets.[9] For these measurements the anode was not coated with CD_2, and the proton energy was assumed to be the deuteron energy measured by neutron TOF on similar shots. Proton-current densities at peak power were 30–50 kA/cm² for planar diodes and about 200 kA/cm² for spherical diodes without correction for enhanced proton-energy deposition. An increase in these values can be expected after correction for enhanced stopping. For the energy-loss measurements, deuteron-current densities were scaled from these results using the measured ion currents, and uncertainies of ± 30% were assigned to the values obtained.

The ion energy loss is expected to deviate from that in cold matter when the stopping medium is a dense plasma of significant ionization.[1-3] Variation of the average ionization (Z) with internal energy per gram (e) for aluminum and polyethyl-

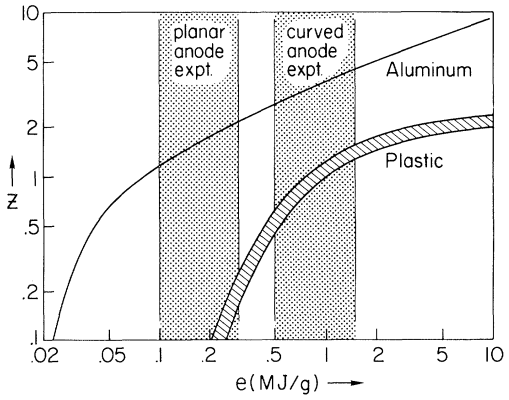

FIG. 5. Dependence of the average ionization on internal energy per gram for aluminum and CH_2 (plastic).

ene (CH_2) from equation-of-state tables[10] is shown in Fig. 5. It is assumed that ionization in Mylar is similar to that in CH_2. The ranges of internal energy per gram corresponding to the experimental conditions are also indicated, where 75% of the deposited energy is converted into internal energy. This partition is determined from hydrocode calculations (to be discussed). The measured deuteron stopping is enhanced [Figs. 4(b)–4(d)] when $Z \gtrsim 1$ from Fig. 5, and is near the cold-target values [Fig. 4(a)] when the ionization is predicted to be low.

Scaling of the stopping power with target ionization can be expressed[3] as

$$S = B[(1 - Z/Z_a)\ln\Lambda_b + (Z/Z_a)\ln\Lambda_f] \quad (1)$$

for a plasma of atomic number Z_a. The quantities $B = 4\pi e^4 N Z_a / mV^2$ and $\Lambda_b = 2mV^2/I_z$ are for nonrelativistic hydrogenic ions. The atomic density of the plasma is N, m is the electron mass, and V is the ion velocity. The average ionization energy for bound electrons (I_z) is Z dependent.[1] The equivalent quantities for free electrons are $\Lambda_f = 2mV^2/I_f$ and $I_f = e^2/\lambda_D$, where λ_D is the plasma Debye length. For target conditions in the present experiment, thermal-electron corrections to Eq. (1) are negligible. For a cold target, $S = S_0$, $I_z = I_0$, $Z = 0$, and $\Lambda_0 = 2mV^2/I_0$ so that

$$\ln\Lambda_0 (S - S_0)/S_0 = (Z/Z_a)\ln(I_z/I_f) - \ln(I_z/I_0). \quad (2)$$

The right side of Eq. (2) depends only on the plasma state and is plotted in Fig. 6 against e for aluminum at $\rho = 0.02$ g/cm^3. This is the Al density at peak power based on hydrocode calculations to be discussed. The left side of Eq. (2), evaluated from Figs. 4(b) and 4(d), is also plotted with experimental uncertainties. This comparison of experimental results with calculated ion-stopping enhancement confirms the ionization scaling of Eq. (1).

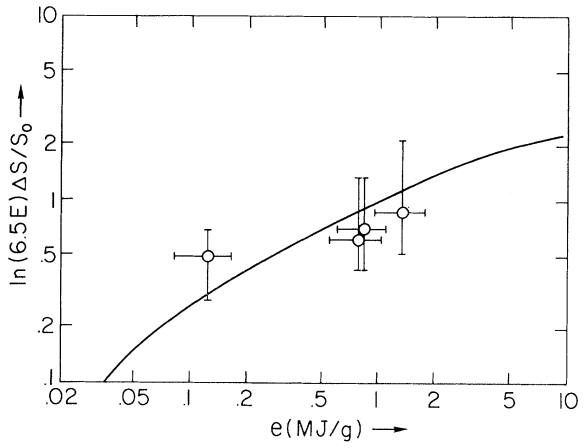

FIG. 6. Comparison of theory and experiment for the dependence of enhancement, $\Delta S/S_0 = (S - S_0)/S_0$, on internal energy per gram for aluminum.

The energy loss of deuterons in the experimental targets was evaluated more precisely by hydrocode simulation with experimental parameters and enhanced stopping.[1] Power on target versus time was based on diode-voltage traces normalized to deuteron energies determined from neutron TOF and ion-current traces normalized to peaks of 50 kA/cm^2 (planar diode) or 250 kA/cm^2 (spherical diode). Target heating was evaluated for a 50-50 mixture of protons and deuterons in the beam based on experimental measurements. These calculations indicate that at peak power, the target has expanded in thickness to about 1 mm at 50 kA/cm^2 and 2 mm at 250 kA/cm^2. In aluminum (Mylar) at peak power, the electron temperature is 4–5 eV (2.5–3.5 eV) at 50 kA/cm^2 and 13–17 eV (9–11 eV) at 250 kA/cm^2. Code-calculated energy losses at peak power, plotted in Fig. 4, agree with most measurements.

In summary, we report measurements of enhanced stopping of ions in dense plasmas. The stopping power of 1-MeV deuterons in aluminum is enhanced by 20% at the 50 kA/cm^2 level and by 40% at the 250 kA/cm^2 level. For Mylar, the stopping power is enhanced by about 45% at the higher current density, but is consistent with cold-target stopping at the lower current density. These results agree with a model of ion-energy deposition which includes stopping by free electrons and the remaining bound electrons in the target.

The work was supported by the U. S. Defense Nuclear Agency and the U. S. Department of Energy.

[a]Permanent address: JAYCOR, Inc., Alexandria, Va. 22304.

[1]T. A. Mehlhorn, J. Appl. Phys. 52, 6522 (1981).

[2]E. Nardi, E. Peleg, and Z. Zinamon, Appl. Phys. Lett. 39, 46 (1981).

[3]D. Mosher, in Proceedings of the U. S. Energy Research and Development Administration Summer Study of Heavy Ions for Inertial Fusion, 1976, Lawrence Berkeley Laboratory Report No. 5543 (unpublished).

[4]G. Cooperstein, Shyke A. Goldstein, D. Mosher,

R. J. Barker, J. R. Boller, D. G. Colombant, A. Drobot, R. A. Meger, W. F. Oliphant, P. F. Ottinger, F. L. Sandel, S. J. Stephanakis, and F. C. Young, in *Laser Interaction and Related Phenomena*, edited by H. Schwarz, H. Hora, M. Lubin, and B. Yaakobi (Plenum, New York, 1981), Vol. 5, p. 105.

[5]Shyke A. Goldstein, G. Cooperstein, Roswell Lee, D. Mosher, and S. J. Stephanakis, Phys. Rev. Lett. 40, 1504 (1978).

[6]F. C. Young, S. A. Goldstein, S. J. Stephanakis, and D. Mosher, in *IEEE International Conference on Plasma Science, Santa Fe, 18–20 May 1981* (IEEE, New York, 1981).

[7]H. Liskien and A. Paulsen, At. Data Nucl. Data Tables 15, 57 (1975).

[8]H. H. Andersen and J. F. Ziegler, *The Stopping and Ranges of Ions in Matter* (Pergamon, New York, 1977), Vol. 3.

[9]R. D. Bleach, D. J. Nagel, D. Mosher, and S. J. Stephanakis, J. Appl. Phys. 54, 3064 (1981).

[10]B. I. Bennett, J. D. Johnson, G. I. Kerley, G. T. Rood, Los Alamos Scientific Laboratory Report No. 7130, 1978 (unpublished). Also data for CH_2 were provided by Andrew Wilson using the CAPO code.

Synchrotron X-Ray Study of Novel Crystalline-*B* Phases in Heptyloxybenzylidene-Heptylaniline (7O.7)

J. Collett, L. B. Sorensen, and P. S. Pershan
Division of Applied Sciences, Harvard University, Cambridge, Massachusetts 02138

and

J. D. Litster and R. J. Birgeneau
Department of Physics, Massachusetts Institute of Technology, Cambridge, Massachusetts 02139

and

J. Als-Nielsen
Risø National Laboratory, DK-4000 Roskilde, Denmark

(Received 10 May 1982)

This paper reports an x-ray diffraction study of structures and restacking transitions within the *B* phases of heptyloxybenzylidene-heptylaniline. The system evolves from a hexagonal close-packed structure, through intermediate orthorhombic and monoclinic phases, to a simple hexagonal structure. The monoclinic phase has a temperature-dependent shear which transforms the system from orthorhombic to hexagonal. The latter three phases exhibit a single-$\vec{q}$ sinusoidal modulation of the molecular layers.

PACS numbers: 61.30.Eb, 64.70.Ew, 81.30.Hd

The realization that an infinitesimally weak interlayer coupling will induce three-dimensional (3D) long-range order in a stack of two-dimensional (2D) crystals has altered our view of the phases previously identified as ordered smectics.[1] Many phases classified as smectic *B* actually are layered molecular crystals (crystalline *B*) with unusual features which are as yet both poorly characterized and barely understood. X-ray diffraction experiments show strong diffuse scattering due to modes polarized in the plane of the layers. This scattering has intralayer correlation lengths greater than 3000 Å but has little interlayer correlation.[2,3] This indicates that layers slide rigidly over one another with relative ease. A second feature is the presence of restacking transitions in which there are dramatic shifts in the relative positions of adjacent layers.[2,4-7] No latent heat or other thermal anomaly has been associated with these transitions, leaving their detailed nature a mystery. It is also not known whether the restacking transition is driven by the interlayer coupling or if it arises from a transition occurring within the individual 2D layers. These crystalline-*B* solids thus represent prototypes of 3D systems with unusually large directional anisotropy. We expect that elucidation of their properties will enhance generally our understanding of crossover from 2D to 3D collective behavior.

High-resolution x-ray diffraction studies of freely suspended thick films of heptyloxybenzylidene-heptylaniline (7O.7) were carried out by using synchrotron radiation and the triple-axis

